J. Fluid Mech. (1983), *vol.* 132, *pp.* 145–162
Printed in Great Britain

Instabilities of dynamic thermocapillary liquid layers. Part 2. Surface-wave instabilities

By MARC K. SMITH† AND STEPHEN H. DAVIS
Department of Engineering Sciences and Applied Mathematics, The Technological Institute, Northwestern University, Evanston, Illinois 60201

(Received 7 October 1982 and in revised form 18 January 1983)

A planar liquid layer is bounded below by a rigid plate and above by an interface with a passive gas. A steady shear flow is set up by imposing a temperature gradient along the layer and driving the motion by thermocapillarity. This dynamic state is susceptible to surface-wave instabilities that couple the interfacial deflection to the underlying shear flow. These instabilities are found to be directly related to the two-dimensional waves on an isothermal layer subject to wind shear as described by Miles and by Smith & Davis. Hence the surface-tension gradients are important only in that they drive the basic shear flow. The surface-wave stability characteristics for liquid layers with and without return-flow profiles are presented, and special attention is paid to long-wave instabilities. Comparisons are made with available experimental observations.

1. Introduction

In Part 1 of this work (Smith & Davis 1983, hereinafter refered to as SD) we formulated models for thermocapillary dynamics in thin two-dimensional liquid layers. We then analysed the convective instabilities of such flows and found both stationary Marangoni convection (as longitudinal roll cells) and a new class of instabilities in the form of travelling hydrothermal waves. These waves are of a thermal origin and are present even when surface deflection is absent. In the present work we focus on surface-wave instabilities in the same model layers.

The surface-wave instabilities we find are travelling waves that couple surface deflections with the underlying bulk shear flow. They are closely related to the instabilities sustained by isothermal liquid layers subject to prescribed wind stresses as analysed by Miles (1960) and Smith & Davis (1982). Thus the imposed temperature gradient and consequent surface-tension gradient drive the basic shear flow but have little effect on the surface-wave instabilities. The present work addresses only two-dimensional instabilities even though Squire's theorem does not hold in the present non-isothermal flow.

Finally, we combine the results of SD with the present work and discuss the preferred mode of instability present in thermocapillary layers. The results of the calculations are compared with available experimental observations.

† Present address: Department of Mathematics, Massachusetts Institute of Technology, Cambridge, Massachusetts 02139.

2. Problem formulation

2.1. *The mathematical model*

We wish to consider the same physical system as in SD in which a liquid layer of mean depth d undergoes motions due to thermocapillarity on its liquid–gas interface. We use the same model, the same notation and the same scalings under which the following dimensionless groups arise: the Reynolds number R, Prandtl number Pr, surface Biot number B and the surface-tension number S. Unlike SD, we restrict ourselves to two-dimensional flows so that we have (non-dimensional) Cartesian coordinates (x, z) with corresponding velocities (u, w). However, we allow significant deflection of the interface located at $z = 1+\eta(x,t)$. This surface has the following unit normal and tangential vectors:

$$\boldsymbol{n} = (-\eta_x, 1)/N, \tag{2.1a}$$

$$\boldsymbol{t} = (1, \eta_x)/N, \tag{2.1b}$$

where

$$N = (1+\eta_x^2)^{\frac{1}{2}}. \tag{2.1c}$$

The alphabetic subscripts denote partial differentiation.

On the free surface the normal stress balances the surface tension times curvature, and the tangential stress balances the gradient of surface tension along the interface. This can be expressed through the following vector equation:

$$\sigma_{ij} n_j = n_i[(SR^{-1}-T)\kappa(\eta)] - t_i[T_{,j} t_j] \quad \text{on} \quad z = 1+\eta(x,t). \tag{2.2a}$$

Here σ_{ij} is the stress tensor of the liquid,

$$\sigma_{ij} = -p\delta_{ij} + e_{ij}, \tag{2.2b}$$

defined in terms of the pressure p and the shear-rate tensor

$$e_{ij} = v_{i,j} + v_{j,i}, \tag{2.2c}$$

$\kappa(\eta)$ is twice the mean curvature of the free surface,

$$\kappa(\eta) = \eta_{xx}/N^3, \tag{2.2d}$$

$SR^{-1}-T$ is the surface tension of the interface, and the last term in (2.2a) represents the gradient in sufrace tension along the interface in the tangential direction. Commas denote spatial differentiation, δ_{ij} is the Kronecker delta and the summation convention is used over the range $i = 1, 3$. The bounding gas is passive with a constant pressure taken equal to zero. The kinematic condition on the free surface is written as

$$w = \eta_t + u\eta_x \quad \text{on} \quad z = 1+\eta(x,t). \tag{2.3}$$

The equality of heat flux at the free surface between the layer and the bounding gas requires

$$-T_{,i} n_i = B(T-T_\infty) + Q \quad \text{on} \quad z = 1+\eta(x,t). \tag{2.4}$$

Here T_∞ is the temperature of the bounding gas far from the interface and Q is an imposed heat flux to the surrounding environment that is determined by the particular basic-state solution under consideration. Note that Q is not an independent parameter.

On the rigid plane there is no slip and zero heat flux:

$$v_i = 0 \quad \text{on} \quad z = 0, \tag{2.5}$$

$$\frac{\partial T}{\partial z} = 0 \quad \text{on} \quad z = 0. \tag{2.6}$$

The governing equations for the liquid layer are the Navier–Stokes equations, the energy equation and the continuity equation:

$$R\left[\frac{\partial v_i}{\partial t}+v_j v_{i,j}\right]=-p_{,i}+\nabla^2 v_i, \tag{2.7a}$$

$$RPr\left[\frac{\partial T}{\partial t}+v_i T_{,i}\right]=\nabla^2 T, \tag{2.7b}$$

$$v_{i,i}=0. \tag{2.7c}$$

2.2. *The basic states*

We consider the same parallel-flow solutions to (2.1)–(2.7) as do SD. These are the linear-flow solution and the return-flow solution. They can be combined as follows:

$$\bar{u}=\bar{u}'(1)z+\tfrac{1}{2}\bar{u}''(1)(z^2-2z), \tag{2.8a}$$

$$\bar{w}=0, \tag{2.8b}$$

$$\bar{p}_x=\bar{u}''(1), \tag{2.8c}$$

$$\bar{T}=-\bar{u}'(1)x+RPr\,\bar{u}'(1)\{\tfrac{1}{24}\bar{u}''(1)(1-z^4)+\tfrac{1}{6}[\bar{u}'(1)-\bar{u}''(1)](1-z^3)\}, \tag{2.8d}$$

$$\bar{\eta}=0, \tag{2.8e}$$

$$\bar{T}_\infty=-x, \tag{2.8f}$$

$$\bar{Q}=-\bar{T}_z|_{z=1}. \tag{2.8g}$$

The unit normal and tangential vectors to the free surface are given as

$$\boldsymbol{N}=(0,1)\equiv \boldsymbol{n}|_{\eta_x=0}, \tag{2.8h}$$

$$\boldsymbol{T}=(1,0)\equiv \boldsymbol{t}|_{\eta_x=0}. \tag{2.8i}$$

When $\bar{u}'(1)=1$ and $\bar{u}''(1)=0$ we obtain the linear-flow solution. When $\bar{u}'(1)=1$ and $\bar{u}''(1)=\frac{3}{2}$ we obtain the return-flow solution.

The linear-flow solution is again exact, while the return-flow solution now represents only an approximate core flow valid for slot aspect ratio $A\to 0$. Sen & Davis (1982) show that this core flow is a valid approximate solution only if

$$S^{-1}=O(A^4) \quad \text{as} \quad A\to 0. \tag{2.9}$$

Thus the surface tension must be very large to sustain a nearly parallel flow in the slot. See SD, §2.2, for further discussion.

2.3. *The linearized disturbance equations*

In a standard way we apply infinitesimal two-dimensional disturbances, denoted by primes, to the system defined by (2.1)–(2.7). After substitution into the governing equations and boundary conditions, we linearize the system and obtain the following linear disturbance equations:

$$R\left[\frac{\partial v_i'}{\partial t}+\bar{u}\frac{\partial v_i'}{\partial x}+\frac{\mathrm{d}\bar{u}}{\mathrm{d}u}w'T_i\right]=-p'_{,i}+\nabla^2 v_i', \tag{2.10a}$$

$$RPr\left[\frac{\partial T'}{\partial t}+\bar{u}\frac{\partial T'}{\partial x}+\frac{\partial \bar{T}}{\partial x}u'+\frac{\partial \bar{T}}{\partial z}w'\right]=\nabla^2 T', \tag{2.10b}$$

$$v'_{i,i}=0, \tag{2.10c}$$

$$v_i' = \frac{\partial T'}{\partial z} = 0 \quad \text{on} \quad z = 0, \tag{2.10d, e}$$

$$w' = \eta_t' + \bar{u}(1)\,\eta_x' \quad \text{on} \quad z = 1, \tag{2.10f}$$

$$\sigma_{ij}' N_j = \left\{(SR^{-1} - \bar{T})\,\eta_{xx}' + 2\frac{\mathrm{d}\bar{u}}{\mathrm{d}z}\eta_x'\right\} N_i - \left\{\frac{\mathrm{d}^2\bar{u}}{\mathrm{d}z^2}\eta' + \frac{\partial \bar{T}}{\partial z}\eta_x' + \frac{\partial T'}{\partial x}\right\} T_i \quad \text{on} \quad z = 1, \tag{2.10g}$$

$$-\frac{\partial T'}{\partial z} - \frac{\partial^2 \bar{T}}{\partial z^2}\eta' + \frac{\partial \bar{T}}{\partial x}\eta_x' = B\left[\frac{\partial \bar{T}}{\partial z}\eta' + T'\right] \quad \text{on} \quad z = 1. \tag{2.10h}$$

We cannot at this stage introduce normal modes to simplify (2.10) because of the appearance of the term $SR^{-1} - \bar{T}|_{z=1} = SR^{-1} + \bar{u}'(1)\,x$ in the normal component of the surface-stress boundary condition (2.10g). This term represents the change in surface tension along the interface due to the linear temperature field in the x-direction and the linear change in surface tension with temperature. If the surface tension does not change much over the characteristic wavelength of a disturbance λ, i.e. if

$$\lambda \ll SR^{-1}, \tag{2.11}$$

then we can approximate the term $SR^{-1} + \bar{u}'(1)\,x$ in (2.10g) by SR^{-1}. In this approximation, we suppress any effect that the variable surface tension might have in the normal-stress boundary condition.

In an alternative approximation, we take the derivative with respect to x of the normal component of the surface-stress boundary condition (2.10g) such as one would do to eliminate the pressure term.

We obtain

$$-\left.\frac{\partial \bar{T}}{\partial x}\right|_{z=1} \eta_{xx}' + [SR^{-1} - \bar{T}|_{z=1}]\,\eta_{xxx}' + 2\frac{\mathrm{d}}{\mathrm{d}z}\bar{u}(1)\,\eta_{xx}'. \tag{2.12}$$

The variable surface tension gives rise to a normal-stress gradient, i.e. $-\partial \bar{T}/\partial x|_{z=1}\,\eta_{xx}'$, that does not vary linearly in x. If the approximation (2.11) is made now, we can neglect the linearly varying part of the surface tension and obtain the following equivalent form of the normal-stress boundary condition:

$$\sigma_{ij}' N_j = \left\{SR^{-1}\eta_{xx}' + \left(2\frac{\mathrm{d}\bar{u}}{\mathrm{d}z} - \frac{\partial \bar{T}}{\partial x}\right)\eta_x'\right\} N_i - \left\{\frac{\mathrm{d}^2\bar{u}}{\mathrm{d}z^2}\eta' + \frac{\partial \bar{T}}{\partial z}\eta_x' + \frac{\partial T'}{\partial x}\right\} T_i \quad \text{on} \quad z = 1. \tag{2.10i}$$

This second approximation is the one employed in the present analysis.

We can now introduce a disturbance system function ψ defined by

$$u' = \psi_z, \quad w' = -\psi_x, \tag{2.13a, b}$$

and normal modes defined as

$$[\psi(x,z,t), p'(x,z,t), T'(x,z,t), \eta'(x,t)] = (\phi(z), P(z), \theta(z), \hat{\eta})\exp[\mathrm{i}\alpha(x - ct)], \tag{2.14}$$

where $\alpha = 2\pi/\lambda > 0$. The complex eigenvalue

$$c = c_{\mathrm{R}} + \mathrm{i}c_{\mathrm{I}} \tag{2.15}$$

consists of the phase speed c_{R} and the growth rate αc_{I} of the disturbances.

The forms (2.13) and (2.14) are substituted into (2.10), where cross-differentiation is used to eliminate $P(z)$, and the kinematic condition (2.10f) is used to eliminate $\hat{\eta}$.

The following Orr–Sommerfeld system is obtained:

$$(\mathrm{D}^2-\alpha^2)^2\phi = \mathrm{i}\alpha R[(\bar{u}-c)(\mathrm{D}^2-\alpha^2)\phi-\bar{u}''\phi], \tag{2.16a}$$

$$(\mathrm{D}^2-\alpha^2)\theta = RPr[\mathrm{i}\alpha(\bar{u}-c)\theta+\bar{T}_x\phi'-\mathrm{i}\alpha\bar{T}_z\phi], \tag{2.16b}$$

$$\phi(0) = \phi'(0) = \theta'(0) = 0, \tag{2.16c, d, e}$$

$$\phi''(1)+\left\{\frac{-\bar{u}''(1)}{\bar{u}(1)-c}-\frac{\mathrm{i}\alpha\bar{T}_z|_{z=1}}{\bar{u}(1)-c}+\alpha^2\right\}\phi(1)+\mathrm{i}\alpha\theta(1) = 0, \tag{2.16f}$$

$$\phi'''(1)-\{\mathrm{i}\alpha R[\bar{u}(1)-c]+3\alpha^2\}\phi'(1)+\left\{\mathrm{i}\alpha R\bar{u}'(1)+\frac{[2\bar{u}'(1)-\bar{T}_x|_{z=1}]\alpha^2}{\bar{u}(1)-c}+\frac{\mathrm{i}SR^{-1}\alpha^3}{\bar{u}(1)-c}\right\}\phi(1) = 0, \tag{2.16g}$$

$$\left\{\frac{-\mathrm{i}\alpha\bar{T}_x|_{z=1}+\bar{T}_{zz}|_{z=1}+B\bar{T}_z|_{z=1}}{\bar{u}(1)-c}\right\}\phi(1)-\theta'(1)-B\theta(1) = 0, \tag{2.16h}$$

where $\mathrm{D} \equiv \mathrm{d}/\mathrm{d}z$, primes also denote $\mathrm{d}/\mathrm{d}z$ and subscripts on $\bar{T}$ denote partial differentiation. The approximation (2.11) can be written in terms of α as

$$\frac{2\pi R}{\alpha S} \ll 1. \tag{2.17}$$

From the solution of (2.16) we obtain the critical values of R and α as functions of S, Pr and B. We then verify *a posteriori* that these values satisfy the inequality (2.17). This check establishes the parameter range in which the theory is reasonable.

As we shall see shortly, the mechanism of the resulting surface mode of instability is a hydrodynamic one. Thus the Reynolds number rather than the Marangoni number is the appropriate parameter to use to predict the onset of the instability.

3. The inviscid problem for the linear flow

Following Miles (1960), we define a reciprocal Weber number

$$W^{-1} \equiv SR^{-2}, \tag{3.1}$$

and examine the leading-order approximation of (2.16) as $R\to\infty$ with W fixed. With the basic-state velocity $\bar{u}(z) = z$ we obtain the following inviscid stability problem from the momentum equation:

$$\phi''-\alpha^2\phi = 0, \tag{3.2a}$$

$$\phi(0) = 0, \tag{3.2b}$$

$$(1-c)\phi'(1)-\phi(1)-\frac{W^{-1}\alpha^2}{1-c}\phi(1) = 0. \tag{3.2c}$$

In this limit the momentum equation (2.16*a*) decouples from the thermal field because the tangential-stress boundary condition (2.16*f*) is dropped. The eigenvalue c which governs the inviscid stability of the thermocapillary layer can be found by solving system (3.2). This system also governs the inviscid stability of the isothermal problem studied by Smith & Davis (1982). Therefore the results of that analysis also apply to the thermocapillary layer, i.e. the layer is inviscidly stable and a sufficient condition for stability as $R\to\infty$ is $W^{-1} \geqslant \frac{1}{3}$ or $R \leqslant (3S)^{\frac{1}{2}}$. For large R then, the stability of the thermocapillary layer is determined by the stability of the isothermal layer.

The thermal field in this limit has two distinct forms depending on the value of the Prandtl number.

3.1. $Pr = 0$

When $Pr = 0$, the thermal field can be solved exactly in terms of the velocity field even without the added condition that $R \to \infty$. The energy equation from (2.10) has the form

$$\nabla^2 T' = 0, \tag{3.3a}$$

$$\frac{\partial T'}{\partial z} = 0 \quad \text{on} \quad z = 0, \tag{3.3b}$$

$$-\frac{\partial T'}{\partial z} + \frac{\partial \bar{T}}{\partial x}\eta'_x = BT' \quad \text{on} \quad z = 1. \tag{3.3c}$$

Using normal modes the solution of (3.3) is

$$T' = \frac{\dfrac{\partial \bar{T}}{\partial x}\cosh \alpha z}{\alpha \sinh \alpha + B \cosh \alpha}\eta'_x. \tag{3.4}$$

In this case, the temperature field is controlled by conduction effects and is forced by a heat flux at the free surface due to the interaction of the horizontal temperature gradient with surface rotation.

3.2. $Pr \neq 0$

When $Pr \neq 0$ and $Pr = O(1)$ as $R \to \infty$, the temperature field is dominated by convection effects. The energy equation reduces to the right-hand side of (2.16*b*). Boundary conditions are dropped so that we can solve from θ from (2.16*b*) and obtain

$$\theta = \frac{\bar{T}_z \phi}{\bar{u} - c} = O(R). \tag{3.5}$$

Here we note that the kinematic condition (2.10*f*) cast in terms of the stream function and normal modes is

$$\hat{\eta} = -\frac{\phi(1)}{\bar{u}(1) - c}. \tag{3.6}$$

On the free surface, the temperature perturbation written in terms of the surface deflection by using (3.5) and (3.6) is

$$T' = -\bar{T}_z \eta' \quad \text{on} \quad z = 1. \tag{3.7}$$

Evaluating the entire temperature field on the free surface and using (3.7) yields

$$T|_{z=1+\eta'} = [\bar{T} + \bar{T}_z \eta' + T']_{z=1} = \bar{T}|_{z=1}. \tag{3.8}$$

Thus, in the limit $R \to \infty$, the free surface of the layer is maintained at its basic-state temperature and no thermocapillary stresses are possible.

4. Method of solution for finite R

We solve the eigenvalue problem (2.16) numerically using a computer code called SUPORT written by Scott & Watts (1975, 1977). This code employs a shooting method, and during the integration process orthonormalization is used to maintain a linearly independent set of solution vectors. In addition, the secant method is used to converge to system eigenvalues.

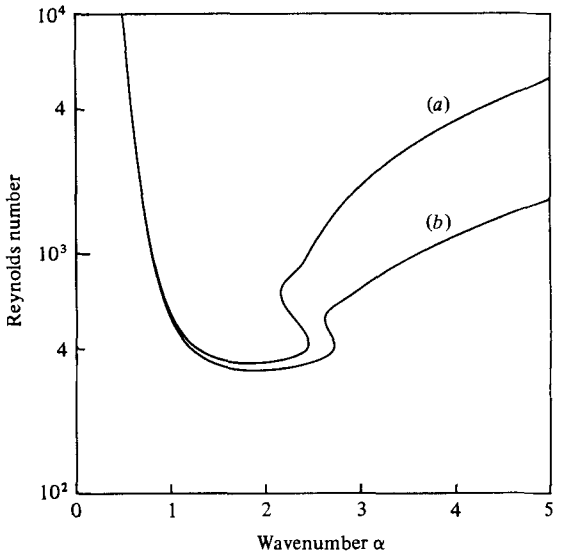

FIGURE 1. Neutral-stability curves for the linear flow with $S = 10^4$. Curve (*a*) is for the isothermal problem of Smith & Davis (1982) and (*b*) is for the thermocapillary layer with $Pr = 0$ and $B = 0$.

5. Results: linear flow

The eigenvalue problem (2.16) is solved for Pr between 0 and 10, B between zero and infinity and S between 10^3 and 10^5. For lower values of S, the critical conditions of the resulting neutral curves violate the inequality (2.17). A typical neutral curve with $Pr = 0$, $B = 0$ and $S = 10^4$ is shown in figure 1. It is compared with a neutral curve from the isothermal problem of Smith & Davis (1982). For $\alpha \to 0$, both curves have the *same* asymptote $R \sim \alpha^{-7}$ as derived by Miles (1960) for the isothermal problem. As α increases the two curves diverge, with the thermocapillary curve lying below the isothermal curve.

The minimum of each neutral curve defines a critical Reynolds number R_c, a critical wavenumber α_c and a critical phase speed c_{Rc} that are functions of the non-dimensional surface-tension number S, the Prandtl number Pr and the Biot number B. The variation of these critical numbers with B is very weak over the entire range of the parameters investigated. Using the value of the critical parameters at $B = 0$ as a reference point, we find that the largest variation in R_c is 6.7%, which occurs for $S = 10^3$, $Pr = 10.0$ and $B = \infty$. For $S \geqslant 10^4$ the change in R_c with B is less than 2% for any Pr. The largest variation in α_c is 5.7%, which corresponds to an absolute change of 0.1 in α occurring at $S = 10^5$, $Pr = 10$ and $B = \infty$. The largest variation in c_{Rc} is 4.7%, which also occurs for $S = 10^3$, $Pr = 10.0$ and $B = \infty$.

With $B = 0$, we find that the changes in R_c, α_c and c_{Rc} as functions of Pr for various values of S are also very weak. Using the value of the critical parameters at $Pr = 0$ as reference point we find that the maximum change in the critical Reynolds number is -7.3%, occurring for $S = 10^3$ and $Pr = 10$. The critical wavenumber has a maximum change of -7.0% at $S = 10^5$ and $Pr = 10$, and the critical phase speed has a maximum change of -5.9% at $S = 10^3$ and $Pr = 10$. For small values of $Pr \leqslant 0.01$, the change of the critical numbers is less than 2% for any S.

Figures 2, 3 and 4 show how R_c, α_c and c_{Rc} vary as functions of the surface-tension number S for $B = 0$ and $Pr = 0.01$. Also shown are the corresponding curves for the isothermal problem from Smith & Davis (1982). Figure 2 shows the stabilizing effect

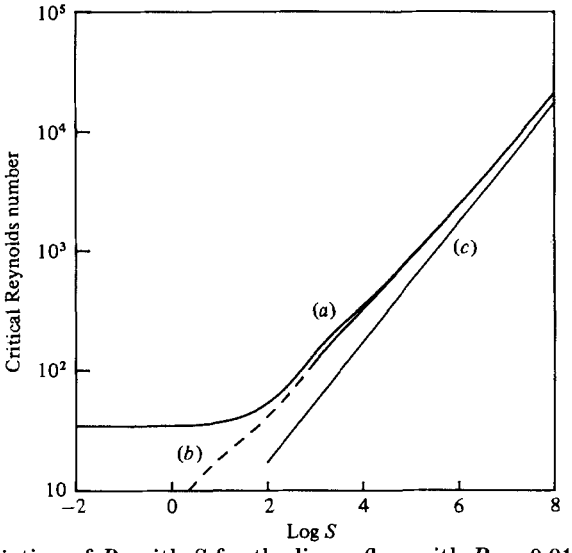

FIGURE 2. The variation of R_c with S for the linear flow with $Pr = 0.01$ and $B = 0$. Curve (a) is for the isothermal problem of Smith & Davis (1982) and (b) is for the thermocapillary layer. Curve (c) is the inviscid limit $R_c = (3S)^{\frac{1}{2}}$. The dashed portion of curve (b) is where the condition (2.17) is not satisfied.

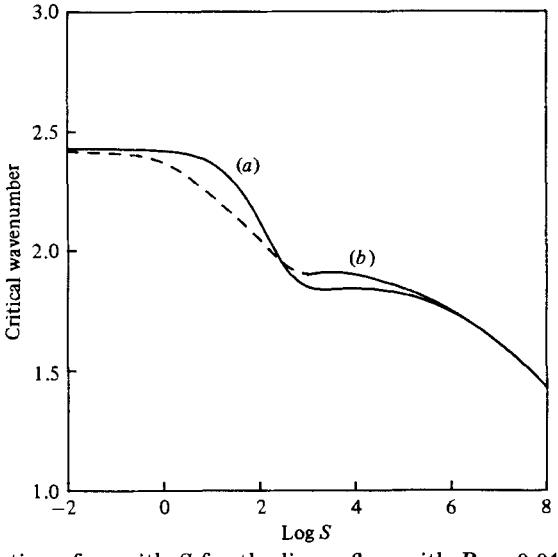

FIGURE 3. The variation of α_c with S for the linear flow with $Pr = 0.01$ and $B = 0$. Curve (a) is for the isothermal problem of Smith & Davis (1982) and (b) is for the thermocapillary layer. The dashed portion of curve (b) is where the condition (2.17) is not satisfied.

of surface tension in that R_c increases with S. For the range of S in which this theory is reasonable R_c for the thermocapillary problem is just a little less than R_c for the isothermal problem. Both curves asymptote to the line $R = (3S)^{\frac{1}{2}}$ for large S because as S increases R_c becomes large and the inviscid limit is approached. Each point on these curves corresponds to a different value of α_c because α_c depends on S as shown in figure 3. As S increases, the surface becomes 'stiffer' and therefore more resistive to short-wavelength corrugations. This accounts for the generally decreasing behaviour of α_c with increasing S. For the range of S in which this theory is reasonable, the

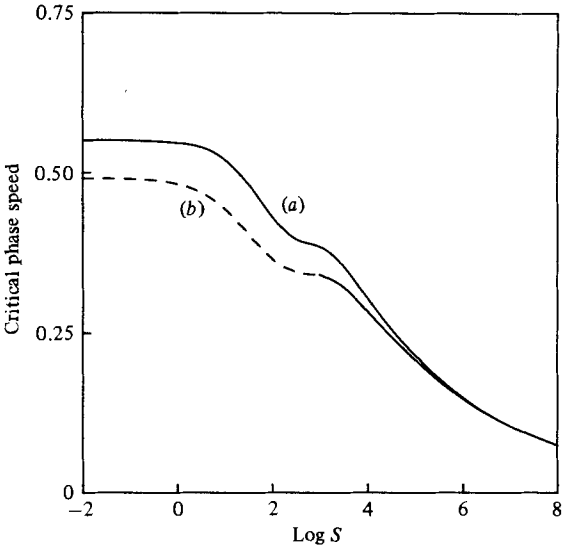

FIGURE 4. The variation of c_{Rc} with S for the linear flow with $Pr = 0.01$ and $B = 0$. Curve (a) is for the isothermal problem of Smith & Davis (1982) and (b) is for the thermocapillary layer. The dashed portion of curve (b) is where the condition (2.17) is not satisifed.

critical wavenumber for the thermocapillary problem is always slightly larger than the critical wavenumber for the isothermal problem.

Figure 4 shows that the critical phase speed c_{Rc} decreases with increasing S. As before, for large S the inviscid limit is approached and the decreasing behaviours of α_{c} and c_{Rc} with increasing S are connected through the inviscid relation given by Smith & Davis (1982). The critical phase speed for the thermocapillary problem is always slightly less than the critical phase speed for the isothermal problem.

Often in free-surface problems the application of linear stability theory to experimental observation becomes difficult because the growth rates of the disturbances are so small that the disturbances cannot be sensed until R exceeds R_{c} by an appreciable amount. Hence it is of some interest to have estimates of the growth rates for $R > R_{\mathrm{c}}$.

In our estimates, we let $B = 0$ and fix S, Pr and $\alpha = \alpha_{\mathrm{c}}$. We then allow R to increase through R_{c}. Note that $\alpha = \alpha_{\mathrm{c}}$ does *not* necessarily correspond to the wavenumber with the maximum growth rate for $R > R_{\mathrm{c}}$ even though it does have this property for $R = R_{\mathrm{c}}$. Figure 5 shows αc_{I} versus R for two values of Pr and two values of S. For $R < R_{\mathrm{c}}$, $\alpha c_{\mathrm{I}} < 0$, then it increases with R, vanishes at R_{c}, increases to a maximum and then decreases to zero as $R \to \infty$. This decrease to zero is consistent with the fact that the shear flow is inviscidly stable.

The maximum values of the growth rate are shown in table 1 along with the corresponding value of R at which the maximum occurs. The growth rate as a function of R for these values of S is very similar to the corresponding function in the isothermal problem shown in figure 9 of Smith & Davis (1982). There, for $S = 10^4$ and $\alpha = \alpha_{\mathrm{c}} = 1.85$, the maximum $\alpha c_{\mathrm{I}} = 0.021\,33$ occurs at $R = 501$. Figure 6 gives the corresponding values of the phase speed c_{R} as R is increased. The limiting value of c_{R} for each curve in figure 6 is given in table 1. This value is obtained from the inviscid analysis.

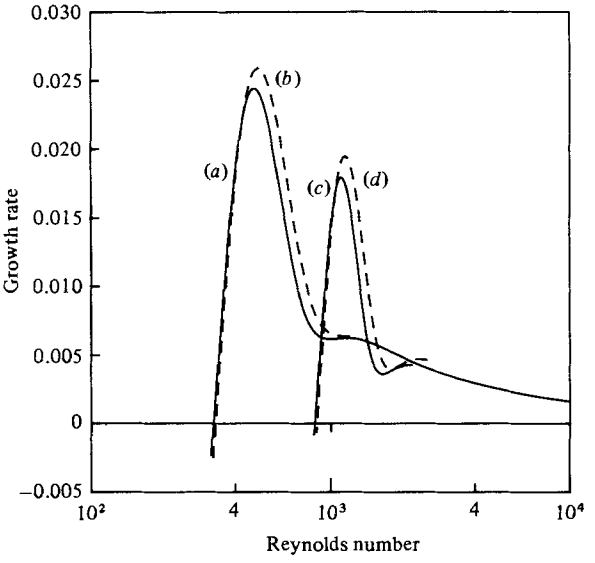

FIGURE 5. The disturbance growth rate for the linear flow versus R. The parameter values and the maximum growth rate associated with each curve are listed in table 1.

Curve	(a)	(b)	(c)	(d)
S	10^4	10^4	10^5	10^5
Pr	0	1.0	0	1.0
α_c	1.91	1.84	1.87	1.76
R_c	324.2	331.5	858.8	876.2
c_{Rc}	0.2825	0.2905	0.2057	0.2151
R_m	478.6	501.2	1122	1148
αc_{Im}	0.02442	0.02592	0.01791	0.01947
$c_{R\infty}$	0.4989	0.4833	0.4901	0.4645

TABLE 1. The parameters associated with the curves in figures 5 and 6. All curves have $B = 0$. Also given are the critical Reynolds number R_c, the critical phase speed c_{Rc}, the maximum growth rate αc_{Im}, the value R_m of the Reynolds number at the maximum growth rate, and the limiting value $c_{R\infty}$ of the phase speed as $R \to \infty$.

6. Long-wave instabilities

Free-surface flows can sometimes exhibit long-wave instabilities at low Reynolds numbers, as shown by Benjamin (1957) and Yih (1963) for film flow down an inclined plane. To investigate the long-wave instability of thermocapillary shear flows we use regular perturbation theory for $\alpha \to 0$, $R = O(1)$, $Pr = O(1)$ and $B = O(1)$ on (2.16). The resulting eigenvalue is

$$c = c_0 + i\alpha[\beta_T R - \tfrac{1}{3}\tilde{S}R^{-1}] + O(\alpha^2), \tag{6.1a}$$

where

$$c_0 = \bar{u}'(1) - \bar{u}''(1), \tag{6.1b}$$

$$\beta_T = -\tfrac{2}{15}c_0\,\bar{u}''(1) - \tfrac{1}{2}c_0\,\bar{u}'(1)\,Pr\,B^{-1}, \tag{6.1c}$$

$$\tilde{S} = \alpha^2 S = O(1). \tag{6.1d}$$

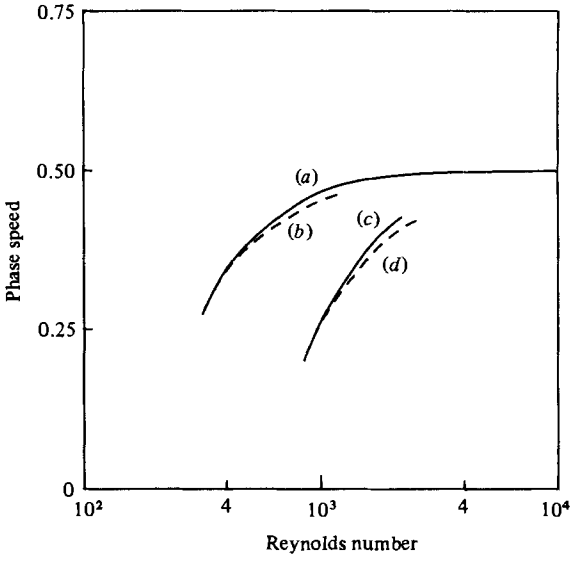

FIGURE 6. The corresponding phase speed for the linear flow versus R. The parameter values and the phase speed as $R \to \infty$ associated with each curve are listed in table 1.

When $\beta_T \leqslant 0$ the system is stable to long waves. When $\beta_T > 0$ the system is unstable to long waves, and the critical Reynolds number is given by

$$R_c = \left(\frac{\tilde{S}}{3\beta_T}\right)^{\frac{1}{2}}, \quad \alpha \to 0. \tag{6.2}$$

Noting that for the basic state we have $\bar{p}_x = \bar{u}''(1)$ and $\bar{T}_x = -\bar{u}'(1)$, we can say the following:

(i) momentum effects are a source of instability when a disturbance travels in the direction of decreasing pressure;

(ii) thermal effects are a source of instability when a disturbance travels in the direction of increasing temperature.

For the linear flow, we find that

$$c_0 = 1, \quad \beta_T = -\tfrac{1}{2} Pr\, B^{-1} \leqslant 0. \tag{6.3}$$

Therefore this velocity profile is stable to long waves, consistent with our numerical calculations. For the return flow, we obtain

$$c_0 = -\tfrac{1}{2}, \quad \beta_T = \tfrac{1}{10} + \tfrac{1}{4} Pr\, B^{-1} > 0. \tag{6.4}$$

Therefore we have a long-wave instability for this velocity profile for all non-zero values of Pr and B. The neutral curve is given by

$$R_c = \{\tfrac{1}{3}\tilde{S}(\tfrac{1}{10} + \tfrac{1}{4} Pr\, B^{-1})^{-1}\}^{\frac{1}{2}}, \quad \alpha \to 0. \tag{6.5}$$

The regular perturbation analysis shows that the temperature perturbation $\theta = O(1)$ for all non-zero values of B. But, when $B = 0$ we find that $\theta = O(\alpha^{-1})$ and that thermal effects influence the leading-order behaviour of the system. For $Pr = 0$ and $B = 0$ the eigenvalue of (2.16) is again expressed by (6.1a) as $\alpha \to 0$, but with

$$c_0 = \bar{u}'(1) - \bar{u}''(1) + \tfrac{1}{2}\bar{T}_x|_{z=1}, \tag{6.6a}$$

$$\beta_T = -[\bar{u}''(1) - \bar{T}_x|_{z=1}]\{\tfrac{2}{15}[\bar{u}'(1) - \bar{u}''(1)] + \tfrac{5}{48}\bar{T}_x|_{z=1}\}. \tag{6.6b}$$

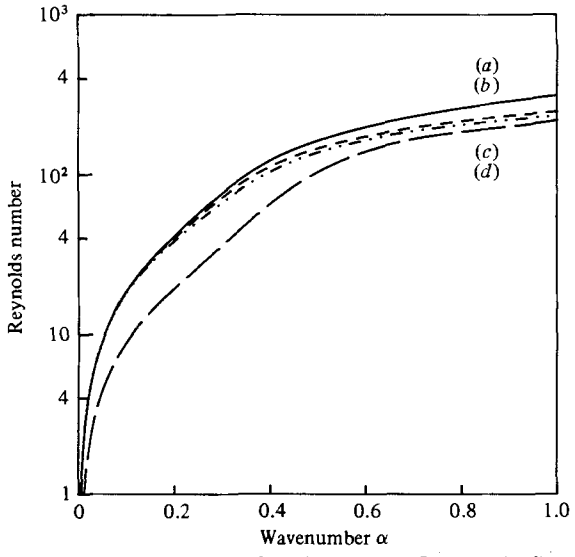

FIGURE 7. The computed neutral curves for the return flow with $S = 10^4$. Curve (a) is for the isothermal problem of Smith & Davis (1982), (b) is for the thermocapillary layer with $B = \infty$ and $Pr = 1$, (c) is with $B = 1$ and $Pr = 0$, and (d) is with $B = 0$ and $Pr = 0$.

For the linear flow we find that

$$c_0 = \tfrac{1}{2}, \quad \beta_T = -\tfrac{7}{240}. \tag{6.7}$$

Therefore this velocity profile is stable to long waves as before. For the return flow we obtain

$$c_0 = -1, \quad \beta_T = \tfrac{41}{96}. \tag{6.8}$$

Therefore this velocity profile has a long-wave instability, with the neutral curve given by

$$R_c = (\tfrac{32}{41}\tilde{S})^{\frac{1}{2}}. \tag{6.9}$$

The critical wavenumber for this instability, $\alpha = 0$, corresponds to a disturbance with an infinitely long wavelength. However, the return flow only exists in a slot of large but finite length. It is reasonable to assume that the slot ends will tend to stabilize those disturbances whose wavelength is larger than the length of the slot. Therefore, to investigate this instability in a range where it is relatively unaffected by the presence of the slot ends, we must extend the analytical results to larger values of the wavenumber.

For the return flow, the neutral curves given by (6.5) and (6.9) were extended numerically to $\alpha = O(1)$ for various values of S, Pr and B. For small α and $\tilde{S} = O(1)$, the numerical results agreed with these equations to $O(\alpha^2)$ accuracy for all values of the parameters considered.

Figure 7 shows numerically computed neutral curves for $S = 10^4$. Curve (a) is for the isothermal layer repeated from figure 14 of Smith & Davis (1982), and curves (b), (c) and (d) are for the thermocapillary layer with $B = \infty$ and $Pr = 1$, $Pr = 0$ and $B = 1$ and $Pr = B = 0$ respectively. For small values of α, curves (a), (b) and (c) agree, as shown by the long-wave analysis.

Figure 8 shows the neutral curves for $S = 10^4$ and for three values of Pr with $B = Pr$. When $Pr = B = 10$, the neutral curve is similar to the $B = \infty$ curve of figure 7. This is evidence of the decreasing sensitivity of the neutral curves on the parameter Pr as B gets large.

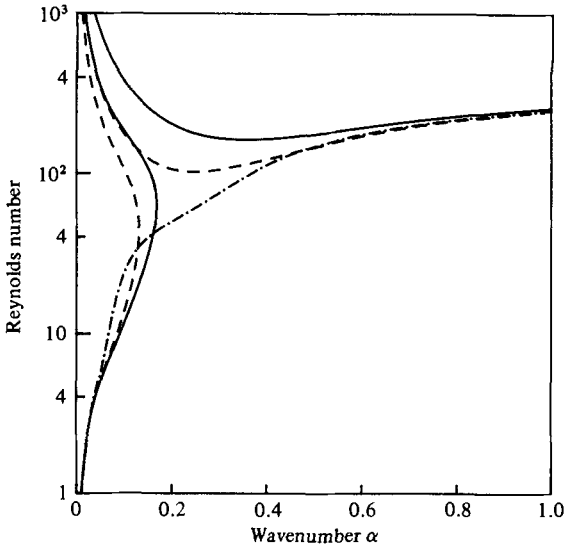

FIGURE 8. The computed neutral curves for the return flow with $S = 10^4$: —·—; $Pr = B = 10$; – – –, $Pr = B = 1.0$; ——, $Pr = B = 0.1$.

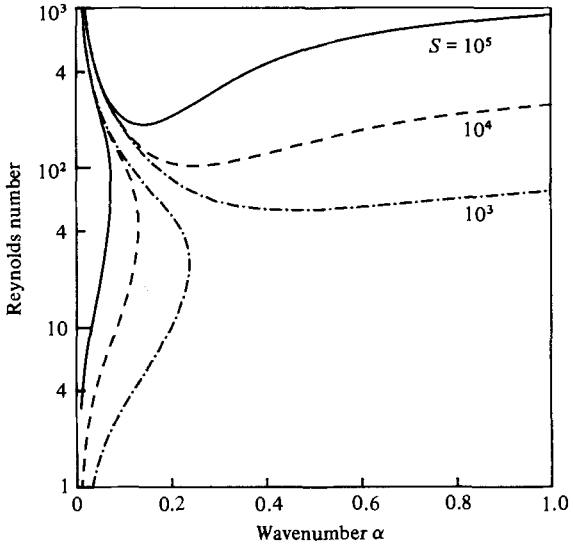

FIGURE 9. The computed neutral curves for the return flow with $Pr = 1$, $B = 1$ and various values of S.

The neutral curves for $Pr = B = 1$ and for three values of $S(= \alpha^{-2}\tilde{S})$ are shown in figure 9. As indicated in the analytical results, we see the stabilization effect of increasing surface tension.

Most of the curves in figures 8 and 9 exhibit a two-branch structure. This structure is investigated in figure 10 for $S = 10^4$ and $B = 0$. When $Pr = 0$, the neutral curve monotonically increases with α. For $Pr = 0.015$, the lower curve has pinched up near $\alpha = 0.3$ and another loop has appeared from above. The interior of this upper loop is a region of stability. These two curves join and form the two-branch structure as shown for $Pr = 0.1$. When $Pr = 1$, we see that the branch that represents the long-wave

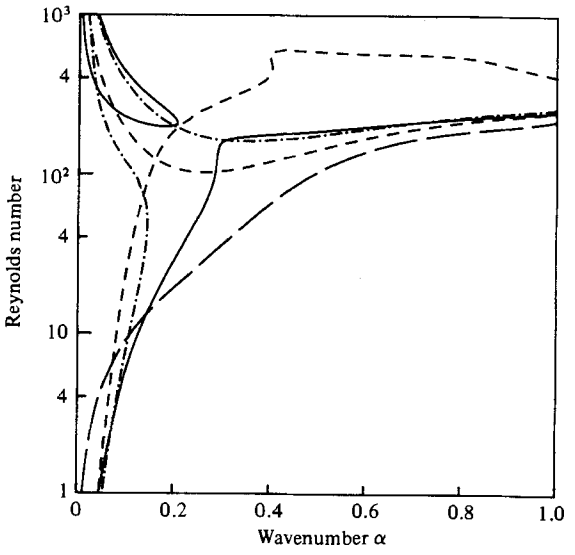

FIGURE 10. The computed neutral curves for the return flow with $S = 10^4$ and $B = 0$: ——, $Pr = 0$; ——, $Pr = 0.015$; —·—, $Pr = 0.1$; – – –, $Pr = 1.0$.

instability moves away from the $\alpha = 0$ axis at large values of R. This branch of the neutral curve is a thermal convection mode of instability that is considered in greater detail in SD.

7. Discussion and conclusions

7.1. *The linear flow*

Because of the restriction (2.17) the stability results for the thermocapillary layer are limited to large values of the surface-tension number S. In this range, figures 2–4 show that the critical values of R, α and c_R are very close to those of the isothermal problem discussed in Smith & Davis (1982). The two problems are related in that as S gets large the critical Reynolds number increases and both problems approach the same limit, i.e. the inviscid limit $R_c = (3S)^{\frac{1}{2}}$.

We have also seen that these critical parameters are relatively insensitive to changes in either the Prandtl number or the Biot number, changing at most by about 7 % with respect to $Pr = 0$ and $B = 0$ over a large range of Pr and B.

In Smith (1982), a disturbance energetics analysis was done on this problem to determine the mechanism of instability. The results of that analysis show that the disturbances receive energy from the mean flow through Reynolds stress and through a normal stress on the interface. These results are very similar to those of Smith & Davis (1982). From this evidence, one can conclude that the instability is adequately approximated by the associated isothermal model described in Smith & Davis (1982) and that the only role of the temperature field is to drive the bulk-fluid motion.

In table 2 we list the critical parameters obtained from this theory in dimensional form for molten silicon at 1410 °C. We consider two layers, one of depth 0.1 cm and one of depth 1.25 cm. With the physical properties of silicon we compute S, and then use figures 2–4 to obtain R_c, α_c and c_{Rc}. For both layers S is large enough so that the condition (2.17) is satisfied indicating that our neglect of the varying surface tension in the normal-stress boundary condition is reasonable. Using these dimensionless critical parameters we compute the following dimensional quantities: the critical

Parameter	Without gravity	Without gravity	With gravity
μ (g cm^{-1} s^{-1})	0.88×10^{-2}	—	—
k (erg s^{-1} cm^{-1} °C^{-1})	0.32×10^{7}	—	—
ρ (g cm^{-3})	2.5	—	—
c_p (erg g^{-1} °C^{-1})	0.84×10^{7}	—	—
σ (dyn cm^{-1})	720	—	—
γ (dyn cm^{-1} °C^{-1})	0.43	—	—
d (cm)	0.1	1.25	1.25
Pr	0.023	—	—
S	2.32×10^{6}	2.91×10^{7}	—
G	7.91×10^{4}	1.54×10^{8}	—
R_c	3350	11700	20900
α_c	1.70	1.53	1.43
c_{Rc}	0.125	0.085	0.075
λ_c (cm)	0.37	5.1	5.5
f_c^* (Hz)	42.3	0.55	0.80
U_c (cm s^{-1})	125	32.9	58.9
c_{Rc}^* (cm s^{-1})	15.6	2.8	4.4
b_c (°C cm^{-1})	25.6	0.54	0.96
$2\pi R_c/\alpha_c S$	0.0057	0.0017	0.0032
$B_0 \alpha_c^{-2}$	0.012	2.3	—

TABLE 2. An application of the theory to a layer of liquid silicon at 1410 °C. The effect of increasing the depth of the layer and of adding gravity are illustrated. The layer has a linear velocity profile.

wavelength λ_c, the critical frequency f_c^*, the critical surface speed U_c, the critical phase speed c_{Rc}^* and the critical temperature gradient b_c. For a layer 0.1 cm in depth the critical temperature gradient is 25.6 °C/cm and the oscillation frequency is 42.3 Hz. Increasing the depth to 1.25 cm stabilizes the layer in that the critical Reynolds number increases by about a factor of 3. However, this also *lowers* the critical temperature gradient to 0.54 °C/cm and the frequency to 0.55 Hz. This linearized mode of instability can be visualized as a wave travelling on the interface of the liquid layer at a speed always less than the interfacial-fluid speed.

Gravity can be included in this model as shown by Miles (1960) by replacing S with $S+G\alpha^{-2}$ in the normal-stress boundary condition (2.16g). Here G is defined as

$$G \equiv gd^3\rho^2/\mu^2, \tag{7.1}$$

where g is the acceleration due to gravity. Gravity can be neglected altogether if $B_0\alpha^{-2} \ll 1$, where B_0 is the Bond number defined as $B_0 \equiv GS^{-1}$. In a silicon layer of depth 0.1 cm, $B_0\alpha^{-2} = 0.012 \ll 1$, and so gravity does not appreciably affect the stability of the system. For a 1.25 cm layer gravitational stabilization is very important, as shown in table 2. The addition of gravity increases the critical Reynolds number by 79%.

In the model presented above we only consider the stabilization effect of gravity on the interface of the liquid layer. Since this is not an isothermal layer, buoyancy forces in the bulk fluid can affect the flow. Since our primary interest is in the instability occurring in the floating-zone process in a microgravity environment, we have *neglected these buoyancy effects.*

7.2. *The return flow*

The condition (2.17) needed for the neglect of the varying surface-tension term in the normal-stress boundary condition is always satisfied in the long-wave analysis. With the scaling used for the surface-tension number S we find that

$$\frac{2\pi R}{\alpha S} = \frac{2\pi R}{\tilde{S}}\alpha. \tag{7.2}$$

This is always much less than unity for long waves with R and $\tilde{S} = O(1)$.

The primary mechanism of energy transfer to long-wave disturbances in the layer is the work done by the tangential stresses on the interface. Through this mechanism thermocapillary stresses can significantly couple into the velocity field and appreciably affect the onset of the instability. In fact, when PrB^{-1} is large the instability is primarily of thermal origin as shown by (6.1) and (6.5).

To eliminate the coupling between the two disturbance fields, thermocapillary stresses at the free surface must be eliminated. This can be done in two different ways. When $Pr = O(\alpha)$, conduction will dominate convection and the layer behaves as a perfect one-dimensional conductor to $O(\alpha)$. When $B \neq 0$, no temperature perturbations are possible and so thermocapillary stresses cannot arise.

For large B the surface temperature is maintained at its basic-state value. Thus thermocapillary stresses on the interface are eliminated directly even though temperature perturbations in the bulk liquid are possible.

In the long-wave analysis of §6, the critical Reynolds number reduces to that of the isothermal problem of Smith & Davis (1982) in both of the above limits. Thus the long-wave instability can be adequately described in the limit of small Pr and/or large B by the corresponding isothermal model.

The stabilization effect of gravity on the interface of the layer can be included in the model by replacing $\tilde{S}$ with $\tilde{S}+G$ in (6.1a) and (6.2). For S fixed and zero gravity, $R_c \to 0$ as $\alpha \to 0$. When gravity is not zero, $R_c = (G/3\beta_T)^{\frac{1}{4}}$ as $\alpha \to 0$. Thus the layer is always stable to long waves for small enough R when gravity is included. This fundamental change in the behaviour of the layer is expected because the condition for the neglect of gravity, i.e. $B_0\alpha^{-2} \ll 1$, is always violated for $B_0 = O(1)$ and $\alpha \to 0$. However, in the micro-gravity environment of space, $B_0 \to 0$, and the results of the long-wave analysis with $G = 0$ will be valid.

As discussed in §6, the long-wave disturbances found to be unstable in the return flow of the slot will be affected by the presence of the slot ends. We can expect these effects to occur when

$$\alpha \leqslant 2\pi A. \tag{7.3}$$

From the restriction of Sen & Davis (1982) that $S^{-1} = O(A^4)$ and our scaling that $S = O(\alpha^{-2})$, we can conclude that the long-wave analysis is only valid for $\alpha < A^2 < 2\pi A$. Thus the analytical result is invalid due to the effect of the end walls. Only by extending these results to larger values of the wavenumber through numerical computation, as shown in figures 7–10, can we describe instabilities that are only weakly affected by the presence of the endwalls.

8. Final comments

In the isothermal problem of Smith & Davis (1982), Squire's theorem proves that a two-dimensional surface wave is always the most dangerous mode. For the thermocapillary layer, Squire's theorem is not valid and so three-dimensional

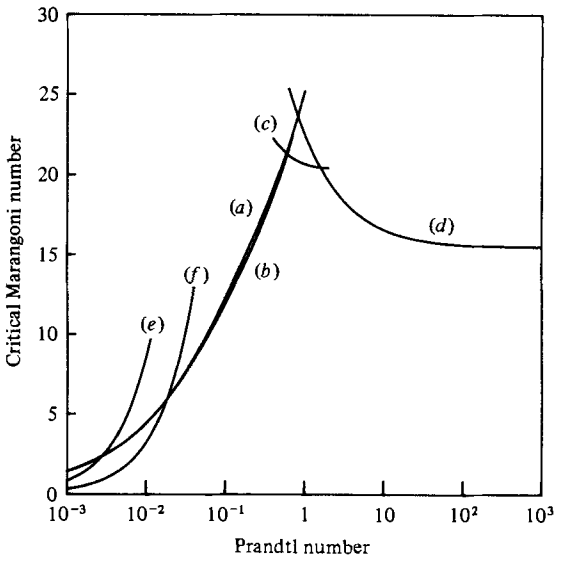

FIGURE 11. The critical Marangoni number M_c versus the Prandtl number for the linear flow with $B = 0$. Curve (a) is for longitudinal hydrothermal waves, (b) is for oblique hydrothermal waves, (c) is for two-dimensional hydrothermal waves, (d) is for longitudinal rolls, (e) is for two-dimensional surface waves with $S = 10^5$, and (f) is for two-dimensional surface waves with $S = 10^4$. The lowest value of M for each Pr defines M_c for the preferred mode.

disturbances cannot be excluded. However, since the form and the mechanism of the surface-wave instability is the same for both of these layers we suppose that the two-dimensional mode will be the most dangerous mode for this instability in the thermocapillary layer. For the return flow, we were able to use regular perturbation theory for small wavenumbers on the normal-mode form of the full three-dimensional disturbance equations to show that a two-dimensional mode does indeed correspond to the most dangerous long-wave disturbance.

We must now compare the results for the surface-wave instability with those of the three-dimensional instabilities of SD so that we can infer the preferred mode of instability as a function of the system parameters.

The three-dimensional thermal instabilities of SD were described in the limit of a non-deformable free surface, i.e. for $S \to \infty$. As S decreases from infinity, the critical Marangoni numbers associated with these modes will decrease slightly. We shall ignore this change in the following comparison.

In figure 11 we repeat the curves of M_c versus Pr for the linear flow from figure 13 of SD and add two more curves corresponding to surface waves at two values of S and $B = 0$. For each of these curves $M_c \sim Pr$ as $Pr \to 0$. Since $M_c \sim Pr^{\frac{1}{2}}$ as $Pr \to 0$ for hydrothermal waves, surface waves will eventually become the preferred instability for small enough Pr. When $S = 10^4$, surface waves are preferred for $Pr < 0.02$, and, when $S = 10^5$, they are preferred for $Pr < 0.003$.

For the return flow in a slot, we expect the slot ends to damp out those disturbances whose wavelength is larger than the slot length. The corresponding neutral curves would have a non-zero minimum unlike those shown in figures 7–10. We can estimate this minimum by using the value of R from our neutral curves that corresponds to a disturbance whose wavelength equals the slot length, i.e. for $\alpha = 2\pi A$. We choose $A = 0.1$ and $S = 10^4$ so that the condition for validity of the return-flow basic-state solution, i.e. $S^{-1} = O(A^4)$, is satisfied. The resulting estimates of the critical Marangoni

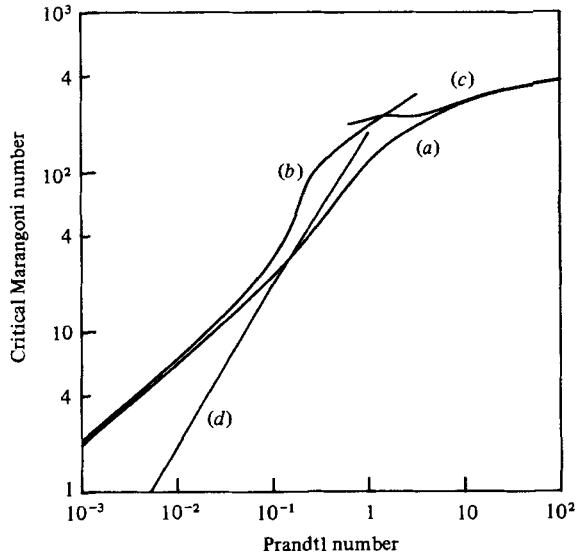

FIGURE 12. The critical Marangoni number M_c versus the Prandtl number for the return flow with $B = 0$. Curve (*a*) is for oblique hydrothermal waves, (*b*) is for longitudinal hydrothermal waves, (*c*) is for two-dimensional hydrothermal waves, and (*d*) is our estimate of M_c for two-dimensional surface waves in the return flow with slot ends for $A = 0.1$ and $S = 10^4$. The lowest value of M for each Pr defines M_c for the preferred mode.

number versus Pr with $B = 0$ are shown in figure 12. Also shown are the corresponding curves for hydrothermal waves from figure 17 of SD. When $Pr < 0.15$, surface waves are preferred.

This crude estimate shows that surface waves are preferred in the slot over a considerable range of Pr. Further estimates for slightly larger A and fixed S indicate that increasing A stabilizes the flow and lowers the value of Pr at which surface waves become preferred. Here we see the importance of the slot ends on the ultimate stability of the flow field to surface waves.

This research was supported through contract no. NAS8-33881, National Aeronautics and Space Administration, Material-Processing-in-Space Program.

REFERENCES

BENJAMIN, T. B. 1957 *J. Fluid Mech.* **2**, 554.

MILES, J. W. 1960 *J. Fluid Mech.* **8**, 593.

SCOTT, M. R. & WATTS, H. A. 1975 *Sandia Labs. Rep.*, SAND75-0198, *Albuquerque.*

SCOTT, M. R. & WATTS, H. A. 1977 *SIAM J. Num. Anal.* **14**, 40.

SEN, A. K. & DAVIS, S. H. 1982 *J. Fluid Mech.* **121**, 163.

SMITH, M. K. 1982 Ph.D. dissertation, Northwestern University.

SMITH, M. K. & DAVIS, S. H. 1982 *J. Fluid Mech.* **121**, 187.

SMITH, M. K. & DAVIS, S. H. 1983 *J. Fluid Mech.* **132**, 119.

YIH, C. S. 1963 *Phys. Fluids* **61**, 321.